RESEARCH ARTICLE

Intensifying ozonation treatment of municipal secondary effluent using a combination of microbubbles and ultraviolet irradiation

Yue Gao[1] · Yutong Duan[1] · Wei Fan[1] · Tiantian Guo[1] · Mingxin Huo[1] · Wu Yang[1] · Suiyi Zhu[1] · Wengang An[1]

Abstract

Ozonation treatment of municipal secondary effluent is complicated by the low solubility of ozone and inefficient production of hydroxyl free radicals from ozone decomposition. To resolve these problems, this study investigated methods for intensifying ozonation treatment, using a combination of microbubbles and ultraviolet (UV) irradiation (UV/MBO). The high efficiency of the method was illustrated by treating river water containing refractory components derived from secondary effluent in a wastewater treatment plant. The results showed that the ozone mass transfer coefficient in a microbubble system was an order of magnitude compared with a conventional macrobubble system at the initial stage. The amount of ·OH generated during the treatment was quantified using a fluorescent probe analysis. The amount of ·OH in the UV/MBO system was almost 2–6 times more than the amount found with conventional ozonation using macrobubbles (CO), CO with UV irradiation (UV/CO), and microbubble ozonation (MBO) units. The UV/MBO system achieved chemical oxygen demand (COD), UV_{254}, and UV_{400} removal performance rates of up to 37.50%, 81.15%, and 94.74% respectively. These levels were 2–36% higher than those in other systems. The coupling UV/MBO treatment significantly reduced all five categories of substances according to EEM spectra and fluorescence regional integration. The distribution of fractions with different molecular weights (MW) was altered and the UV_{254} of MW (< 500 Da) increased by 15.8%. The biodegradability of the water was significantly improved, as indicated by the TOC/UV_{254}. This is ascribed to the enhanced degradation of refractory organics in the water. The combination of the UV/microbubble technique with ozonation could provide an efficient approach for advanced wastewater treatment.

Keywords Secondary effluent · Ozonation · Microbubble · Ultraviolet irradiation · Advanced treatment · Fluorescent probe

Introduction

River water quality deterioration is a serious concern in developing countries and has become increasingly worse with rapid urbanization and inadequate water/wastewater treatment and management over the past decades. In particular, it is common for wastewater treatment plants (WWTPs) to directly discharge secondary effluent (SE) into urban rivers in many cities and towns, leading to seriously polluted river basins (Saeed et al. 2016; Munz et al. 2017). Usually, SE contains a lot of refractory organic pollutants, which do not degrade well during the conventional activated sludge process in WWTPs. After SE is discharged into rivers and estuaries, it can impact aquatic ecosystems and pose potential risks to human health (Xing et al. 2018; Qiao et al. 2018). Therefore, additional effective treatments are needed to purify WWTP effluent and improve the water quality of the receiving urban river.

Ozone is one of the most effective methods for treating refractory species. It is a well-known powerful oxidant, and it has been widely used in reclaimed water treatment (Domenjoud et al. 2011). However, ozone oxidation technology has serious limitations. The lifetime of ozone in water is quite short (the half-life is about 15 min at 298 K at pH = 7) (Cullen et al. 2009), and its low solubility (Ikeura et al. 2011) in water results in a slow reaction rate with pollutants. The ozone oxidation process contains

✉ Wei Fan
fanw100@nenu.edu.cn

Yue Gao
gaoy347@nenu.edu.cn

[1] School of Environment, Northeast Normal University, Changchun 130117, China

direct and indirect pathways. In the direct pathway, the oxidation occurs by means of molecular ozone; in the indirect pathway, oxidation occurs through the action of hydroxyl radicals (·OH) generated by ozone decay (Chiang et al. 2006). In contrast, the hydroxyl radical pathway is non-selective and the radicals with a high standard redox potential (2.8 V) react with most organic compounds occur through H-atom abstraction, direct electron transfer, or insertion. This is unlike molecular ozone, which selectively attacks molecules with high electron density functional groups, including double bonds and aromatic systems (Jin et al. 2012). However, the hydroxyl pathway is not always the main pathway and there is a limited amount of hydroxyl radical generated (Marce et al. 2016). As such, advanced oxidation processes have been highlighted to increase the efficiency of ozonation, based upon the enhanced transformation of ozone into ·OH, which is highly reactive with most inorganic and organic pollutants.

Microbubbles are defined as small bubbles with diameters less than several tens of micrometers (Zimmerman et al. 2011). They have several unique physical properties. These ultrafine bubbles have lower buoyancy, enabling them to slowly rise and providing for a longer residence time in the solution (Parkinson et al. 2008). A decrease in bubble diameter also results in high internal pressure of gas inside the bubble, enhancing the high oxygen mass transfer efficiency (Takahashi et al. 2007). Moreover, microbubbles have a large specific surface area, creating a larger contact surface between the gas and liquid phases. This significantly promotes chemical reactions, physical adsorption, and mass transport in the interface. Further, microbubble collapses can generate a shock wave that generates free radicals. The main reactive oxygen species (ROS) is the hydroxyl radical (·OH) (Liu et al. 2016; Wang et al. 2018). Therefore, we hypothesized that microbubble-aided ozonation could enhance the solubility of ozone in water and contribute to pollutant removal.

Ultraviolet (UV) irradiation is a typical catalytic ozonation method. In the UV/O_3 system, UV irradiation results in a cleavage of dissolved ozone, followed by a fast reaction of atomic oxygen with water (von Sonntag 2008). This forms a thermally excited peroxide (H_2O_2), which then decomposes into two ·OH radicals (Miklos et al. 2018). This process may contribute to pollutant degradation and enhance ozone utilization in the indirect pathway described above. In this study, we developed an intensified ozonation technique, using the combination of microbubbles and UV irradiation to treat contaminated river water fed by SE from a WWTP in Northeastern China. The study used comparative experiments to examine the synergistic effect of microbubbles and UV irrigation on the purification process. Possible mechanisms were then illustrated using hydrochemical analysis and calculations.

Materials and methods

Source and characteristics of the contaminated river water

The contaminated river water for this study was collected from the Yitong River, located in an arid/semi-arid region in Northeastern China. The secondary effluents from several WWTPs were discharged into the river near the urban region (Changchun city); this is one reason for the recent water quality deterioration (Ji et al. 2017). The water samples were collected from the discharge zone of the North WWPT in Changchun. Particulate matter was removed from the water samples by filtering the water through a 0.45-μm filter. This allowed the experiments to focus on removing dissolved organics. After filtration, the basic characteristics of river water samples were assessed. The total dissolved organic (TOC) was 43.79 ± 0.44 mg/L; the COD was 22.50 ± 0.50 mg/L; the total phosphorus was 0.26 ± 0.01 mg/L; and the total nitrogen was 7.40 ± 0.20 mg/L. The initial UV absorbance at wavelength 254 nm (UV_{254}) was 0.119 ± 0.03 and the UV_{400} was 0.018 ± 0.001. The pH varied from 7.61 to 8.25.

### Microbubble/macrobubble generation

Microbubbles were generated using a microbubble generator (Xiazhichun, China). Gas was mixed with liquid and rotated at a high speed in the machine's mixing tank. The high-speed rotation formed a negative pressure cavity in the mixing tank, allowing the gas to be sucked into the generator. The gas was ejected from a special nozzle with liquid. A mass of microbubbles was produced due to great shear force caused by high-speed rotation (Yao et al. 2016). Afterwards, the solution became milky in appearance. A Multisizer 4e counter (Beckman Coulter, USA) was used to measure the number and size of microbubbles in the water.

Macrobubbles were generated using a conventional aerator (Songbao SB718, China). The diffuser diameter was 30 mm and the pore size was ~0.1 mm, based on the manufacturer's instructions. Pictures of the macrobubbles were taken from outside the transparent reactor; these pictures were used to measure the macrobubble diameters.

Generation of ozone and UV irradiation

Ozone was generated using pure oxygen in a corona discharge generator (CH-ZTW7G, China). The oxygen flow rate into the ozonator was maintained at 0.5 L/min, and the ozonation rate was 7 g/h. The applied dosage was adjusted by changing the ozone concentration of ozone, which was controlled by increasing or decreasing the generator's power supply. The UV irradiation was generated using five normal diving UV lamps (Fig. 1), with a low output of 11 W each. The diving

Fig. 1 Experimental schematic and conceptual model
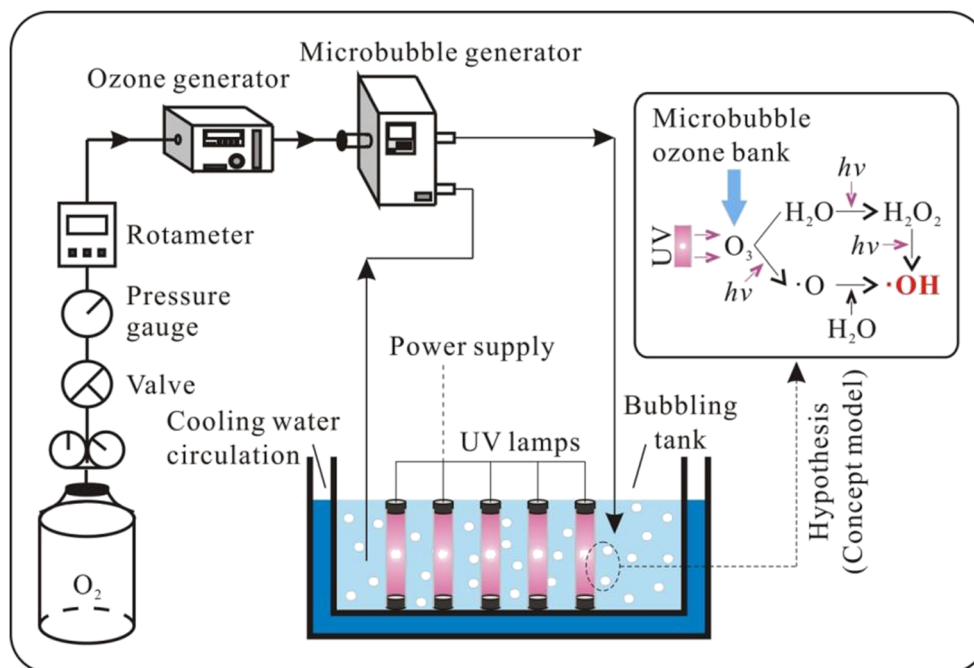
lamp was 23.5 cm long. The UV fluence rate at 13.5 cm from the center of the UV lamp was 40 $\mu W\ cm^{-2}$.

Experimental design

This study included two experiments, run in duplicate to verify the criterion of repeatability. The first experiment explored ozone solubility in water under different aeration scenarios. This allowed an examination of enhanced ozone mass transfer by the microbubbles. To conduct this experiment, a 20-L volume of tap water was stored in the stainless steel reactor (Fig. 1). Microbubbles were continuously generated in the tap water for 30 min, with an oxygen flow rate of 0.5 L/min. The temperature was maintained between 15 and 18 °C using a cooling water circulation system. For comparison, a conventional aerator was used to generate macrobubbles under the same experimental conditions. In the second experiment, the contaminated river water was purified using conventional ozonation with macrobubbles (CO), CO with UV irradiation (UV/CO), microbubble ozonation (MBO), and microbubble ozonation coupled with UV irradiation (UV/MBO). A 20-L water sample was collected from Yitong River and was treated in the same reactor for 30 min. Samples were collected from the reactor using a pipette every 5 min to facilitate analysis. Figure 1 shows the experimental set-up.

Admittedly, the powers of the ozone generator, the microbubble generator, and the UV lumps were up to 130, 550, and 55 (5 × 11) W respectively. According to the current electrovalence (0.54 ¥/kWh) in Changchun city, the energy cost of the UV/MBO experiment (volume—20 L, duration—30 min) in this work is up to 0.20 ¥, roughly 6.62–

9.93 ¥ per ton for 20–30 min's treatment. That means the UV/MBO technique needs large amounts of electrical energy, resulting in relatively high energy demands. However, it covers a wide range of organic reactivity and we supposed that it could be an alternative for advanced treatment of contaminated water due to the high efficiency, and it can be easily equipped in small river courses.

Analytical methods

The temperature and dissolved ozone concentration of the water were recorded automatically every 30 s using a SIN-R200D datalog device (Sinomeasure, China). The water temperature was measured using a Pt100 thermometer. The ozone concentration in the liquid phase was measured using an ozone meter (innoCon 6800CL, UK); the concentration in the gas phase was analyzed using the iodometric method with a potassium iodide solution (Chu et al. 2008). TOC and COD (Cr) were measured using a TOC-L analyzer (Shimadzu, Japan) and DR3900 analyzer (Hach, USA) respectively. The UV absorbance at wavelength 254 nm and 400 nm was measured using a spectrophotometer (GENESYS 10S UV-VIS, Thermo Fisher Scientific, USA). The UV_{254} value was used to reflect the relative content of the aromatic structures and the unsaturated compounds in the water solution. The UV_{400} value was used to examine the decolorization capacity of the ozone process.

An excitation-emission matrix (EEM) was obtained in the excitation wavelength range of 220–450 nm and the emission wavelength range of 280–600 nm at 5-nm intervals (LS-55, PerkinElmer, USA). The areas affected by first- and second-

order Rayleigh and Raman scatter were removed and adjusted by interpolation. Then, the fluorescence regional integration (FRI) technique was adopted to analyze the EEM data and to quantify the proportion of the five regions of excitation/emission, based on a previous study (Chen et al. 2003). The molecular weight (MW) distribution of organic matter in the water sample was measured using a stirred dead-end membrane filtration cell (MSC300, Mosu Corporation, China), installed with a series of polyethersulfone membranes (100 kDa, 50 kDa, 30 kDa, 10 kDa, 3 kDa, 1 kDa, 500 Da) (Zhao et al. 2014). The water was divided into 8 fractions. A 350-mL filtered sample was poured into the stirred ultrafiltration cell, and the cell was placed on the magnetic stirring table. The membrane filtration was driven by pure nitrogen at an operating pressure of 0.05–0.4 MPa, based on the membrane type. Filtration ended when the volume of the residual sample in the cell dropped to 50–100 mL. Finally, the filtrate with lower MW organic matter was collected for further analysis. The UV_{254} value was used to quantitatively indicate the presence of organic substances in different MW solutions.

A fluorescence probe, 3′-p-(aminophenyl) fluorescein (APF), was used to detect the generation of ·OH radicals in the water solution (Wang et al. 2018). The APF itself is non-fluorescent until it reacts with the hydroxyl radical and produces fluorescein that shows bright green fluorescence. Fluorescein has an excitation-emission matrix peak located at an excitation wavelength of 490 nm and an emission wavelength of 515 nm; the peak was measured using a fluorescence spectrophotometer (F97XP, Jingke, China). To quantify the ·OH radicals, we can examine the fluorescence response of APF to different concentrations of H_2O_2 (0 to 1 mM) firstly, and then obtain a linear correlation between the fluorescence intensity and the ·OH concentration produced by H_2O_2 decomposition. If we measured the fluorescence intensity of water sample in the ozonation experiments, we can estimate the quantity of generated ·OH using an equivalent H_2O_2 concentration (Liu et al. 2016; Wang et al. 2018).

The volumetric mass transfer coefficient, K_La, was the product of the liquid-side mass transfer coefficient K_L and interfacial area a. The value can be calculated using Eq. (1) (Zheng et al. 2015):

$$K_L\alpha = \frac{\ln\left(\frac{C_S}{C_S - C_t}\right)}{t} \tag{1}$$

In this expression, C_t (mg/L) is the ozone concentration in the reactor at contact time t and C_S (mg/L) is the dissolved ozone concentration in saturated conditions.

The duplicated experimental data for specific parameters were compared by using Student's t test at the 95% confidence level to examine the experimental reproducibility (Özcan and Özcan 2004). The data array of bubble sizes, pH, COD, TOC,

UV_{254}, UV_{400}, and the amount of ·OH radicals in parallel experiments were evaluated, and the results showed the values of P of abovementioned parameters were 0.30, 0.07, 0.10, 0.22, 0.86, 0.79, and 0.86 correspondingly. There were no significant differences between the duplicated experimental data ($P > 0.05$) (Özcan and Özcan 2004), which indicated that all experiments in this study had good repeatability and high accuracy.
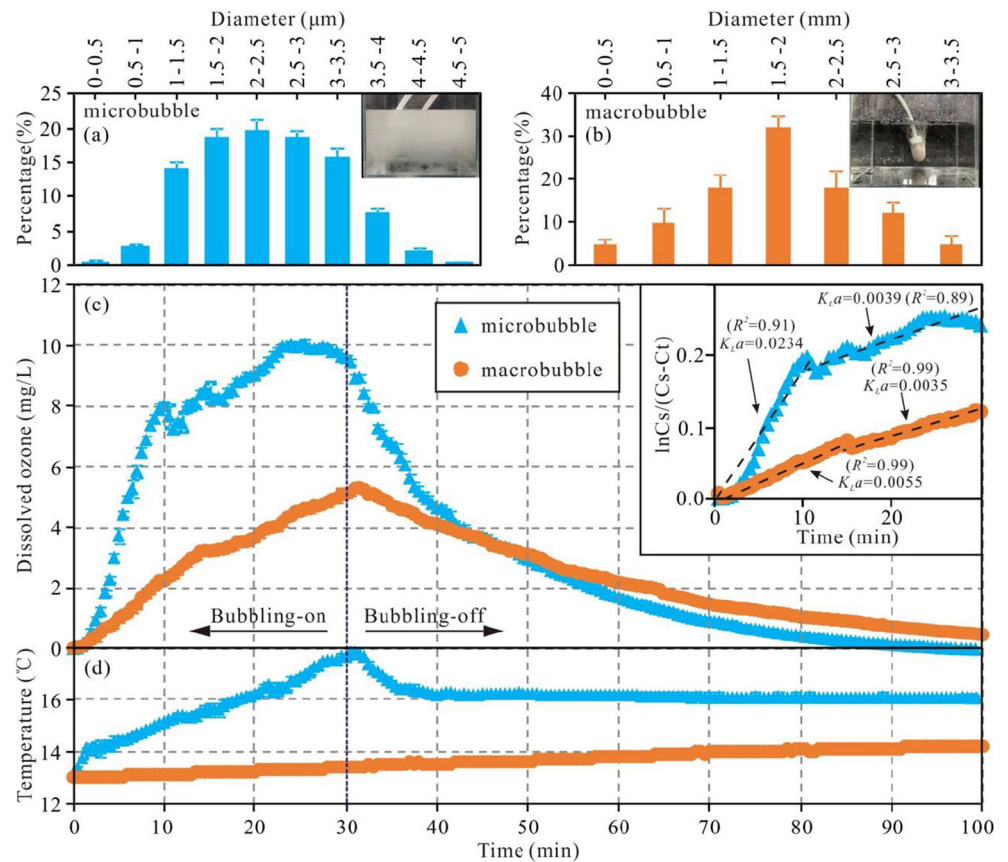
Results and discussion

Basic characteristics of the microbubbles and the enhanced mass transfer of ozone

The mean diameter of the generated microbubbles was 2.35 ± 0.84 μm. The d_{10}, d_{50}, and d_{90} values were 1.26, 2.35, and 3.51 μm respectively. Compared with the macrobubbles produced using a conventional sparger, the mean microbubble diameter was over 1000 times smaller than the mean macrobubble diameter (near 3 mm) (Fig. 2a, b). The speed at which the bubbles rise, which determines their retention time in the water, is mainly related to the bubble size (Parkinson et al. 2008). According to the theoretical values associated with Stokes' law (Parmar and Majumder 2015), the speed at which the microbubbles rose was approximately 1.17×10^6 times slower compared with the macrobubbles. The long stagnation and wide surface area of the microbubbles in the water contributed to its exceptional ability to dissolve gas. Moreover, the Young-Laplace equation demonstrated the interior gas pressure increased as the bubble become smaller (Li et al. 2009), and a high-pressure spot could form during the final stage of bubble collapse. This allowed the gas to dissolve into the water through the gas-liquid interface (Temesgen et al. 2017).

The experimental results support the analysis above. Figure 2 c shows the variations in ozone concentrations under different bubbling scenarios. In all experiments, after the bubbling-on, the ozone concentration increased sharply and then decreased after the bubbling-off. The calculated K_La was divided into two stages during the aeration process using Eq. (1), and the values of the squared correlation coefficient (R^2) were higher than 0.85, which implicated that the data were fitted well and the calculated K_La was reliable. The ozone concentration rose rapidly during the first 10–15 min, because of the large concentration of driving forces. The growth rate then slowed due to the decline in the driving force, as the ozone concentration in the liquid phase increased. In the microbubble system, the K_La was 0.0234 min^{-1} during the first stage (0–10 min), and 0.0039 min^{-1} during the second stage (10–30 min). In the conventional macrobubble system, the K_La was 0.0055 min^{-1} during the first stage (0–15 min), and 0.0035 min^{-1} during the second stage (15–30 min).

During the first stage, the $K_L a$ value in the microbubble system was an order of magnitude larger compared with the value in the macrobubble system. These results show that the microbubble could reach a higher gas transfer rate than the conventional macrobubble. The microbubble efficiently transferred ozone from the gas phase to the liquid phase. After bubbling-off occurred, the ozone concentration of microbubble water was slightly lower (Fig. 2d). This is because the compression activity of the microbubble generator led to higher temperatures. This temperature effect could be avoided when the microbubble generation was performed in a streaming flow unit or in open water (e.g., a river or lake).

Removal of organic matters

Figure 3 shows TOC, COD, UV_{254}, UV_{400}, and TOC/UV_{254} removal levels using the CO, UV/CO, MBO, and UV/MBO treatments. All treatments effectively removed COD and UV absorbance. The final ($t = 30$ min) COD removal rates were $6.67 \pm 1.51\%$, $16.67 \pm 3.55\%$, $27.27 \pm 2.04\%$, and $37.50 \pm 1.31\%$ using CO, UV/CO, MBO, and UV/MBO respectively; COD removal rates with UV_{254} were $50.86 \pm 1.54\%$, $74.19 \pm 1.16\%$, $67.29 \pm 1.47\%$, and $81.15 \pm 1.79\%$ using CO, UV/CO, MBO, and UV/MBO respectively. Like the UV_{254} performance, UV_{400} decreased as a result of each treatment; removal rates reached $58.82 \pm 1.45\%$, $92.86 \pm 2.30\%$, $78.57 \pm$

3.40%, and $94.74 \pm 1.18\%$, using CO, UV/CO, MBO, and UV/MBO respectively. In comparison, between the removal rates of CO and MBO, we can confirm that microbubble contributed 20.72% more to COD reduction, 16.43% more to the reduction of UV_{254}, and 19.75% more to the reduction of UV_{400}. Similarly, the improvements by UV irradiation increased up to 10.11%, 18.60%, and 25.10% for the removal of COD, UV_{254}, and UV_{400} respectively. All of these results indicate that the hybrid system (UV/MBO) was the most efficient. The reduction of UV absorbance, which was strongly linked to the ozone reaction with the unsaturated bonds and the aromatic rings of organic compounds (particularly humic substance), leads to the splitting of bonds and ring dissociation rings according to the Criegee mechanism (Liu et al. 2012).

UV irradiation can lead to the direct excitation of some organic compounds; these excited compounds react with ozone molecules to form different degradable products (Tripathi et al. 2011). Thus, the efficiency of this mechanism would be enhanced by the high concentration of ozone, and the biodegradability could be improved. However, with respect to TOC removal, none of the treatments showed substantial beneficial effects; the TOC removal rates in all experiments were less than 4.0%. As previously reported (Nishiyama et al. 2017), ozone can decompose large molecular matter into low molecular organic compounds, e.g., organic carboxylic acid. However, it was difficult to thoroughly

Fig. 3 Changes of pH, TOC, COD, UV_{254}, and UV_{400} and the ratio of TOC/UV_{254} during CO, UV/CO, MBO, and UV/MBO treatments
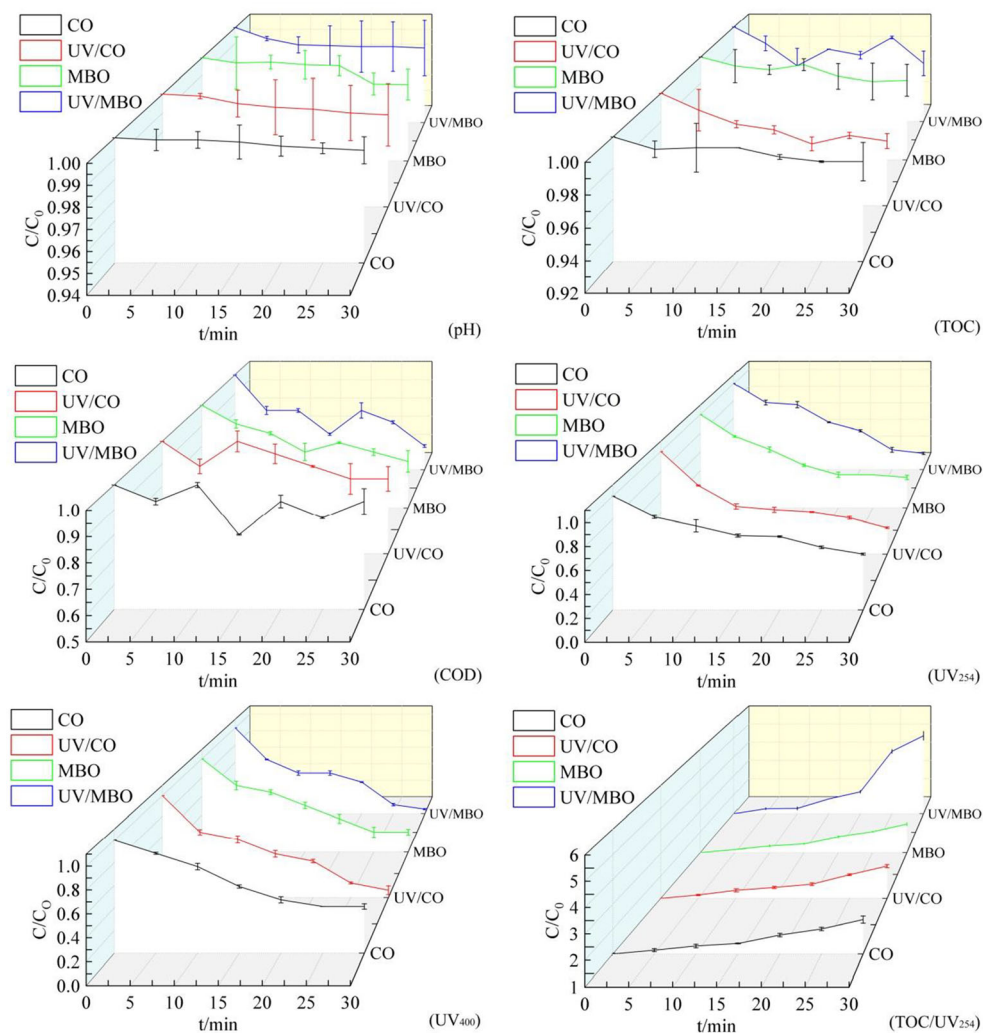

mineralize organic compounds (e.g., CO_2) in a short time. There have also been cases where the refractory organic matter could not be degraded by hydroxyl radicals into organics that were detectable using these measurements (such as TOC) (Baker et al. 1999). During all treatments, the pH values displayed very slight decline, and the values of C/C_0 varied from 1 to 0.984–0.994 as shown in Fig. 3. These negligible variations may attribute to the production of low molecular organic acid mentioned above.

Tambo and Kamei (1978) classified water treatability, finding that water having a TOC/UV_{254} ratio over 30 was suitable for biochemical degradation treatment. This study also adopted TOC/UV_{254} as the index to study river water biodegradability. Figure 3 shows the variations in the TOC/UV_{254} ratios during the experiments. After ozone treatments, river water biodegradability significantly increased with reaction time in all systems. The TOC/UV_{254} ratio increased most quickly and significantly in the UV/MBO system, finally reaching 1860. The integrated ozonation treatment coupling microbubbles with UV irradiation enhanced biodegradability during ozonation.

Molecular weight distribution variation of organic matter

To verify that the ozone could change and destroy the molecular structure, enhance pollutant removal efficiency, and improve biodegradability, we investigated the variations in the MW distribution in the organic matter before and after ozonation. Figure 4 shows the variation in MW with reaction time. Before ozonation, more than 60% of the UV_{254} was in the fraction with MW > 500 Da, and there were many large organic molecules in the raw water. Ozonation led to an increase in the relative proportion of smaller molecules (MW < 500 Da). The proportions of the fraction with MW < 500 Da were approximately $48.78 \pm 2.50\%$, $50.00 \pm 1.48\%$, $42.60 \pm 2.20\%$, and $53.30 \pm 12.80\%$ with the CO, UV/CO, MBO, and UV/MBO treatments, respectively, after 30 min of treatment. This demonstrates that ozonation destroyed the structure of the organic substances in water and could lead to the transformation of large molecules into smaller ones. The UV/MBO

Fig. 4 Fractions of UV$_{254}$ with different molecular weights in raw water and treated samples in the four systems (treated for 30 min): CO, UV/CO, MBO, and UV/MBO
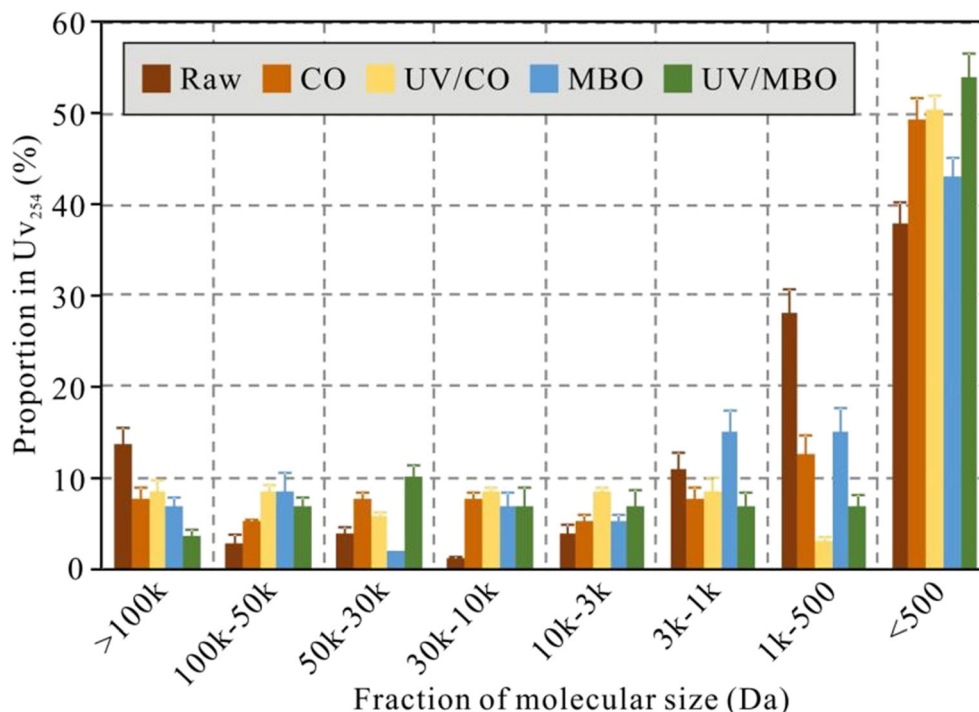
contributed to a more significant increase of low MW molecules in water. This provided benefits for the subsequent advanced treatment.

Evolution of the EEM fluorescence

The EEM spectra, representing a 3-D plot of fluorescence intensity versus excitation and emission wavelengths, reveal the removal rates of different organic substances, including protein-like organic matter (corresponding to an EEM peak at lower excitation/emission wavelengths) and humic-like organic matter (corresponding to an EEM peak at higher excitation/emission wavelengths). There were five different partitions (Fig. 5), based on variable excitations and emissions. The five regions were classified as follows (Chen et al. 2003): region I (tyrosine/tryptophan amino acid region with Ex/Em = 220–250/280–320), region II (tyrosine/tryptophan protein region with Ex/Em = 220–250/320–380), region III (fulvic acid region with Ex/Em = 220–250/380–460), region IV (tryptophan-like or soluble microbial by-product-like material with Ex/Em = 250–380/280–380), and region V (humic acid–like organics with Ex/Em = 250–380/380–460). Based upon the percent fluorescence response (P_i, i is the region) calculated using the FRI method, Fig. 5 shows that the main composition of dissolved organic matter in raw water included fulvic acid ($P_{III} = 0.28$) and humic acid–like organics ($P_V = 0.43$). These results were consistent with the UV$_{254}$ results above.

The fluorescence intensity of the water disappeared gradually in the five regions with reaction time, indicating that ozonation destroyed the structure of organic substances in water. The EEM spectra of the water samples, with corresponding reaction times (10, 20, and 30 min) in the MBO and UV/MBO systems, are specifically shown here to further illustrate performance. It should be pointed out that there was no fluorescence peak in EEM spectra of water samples after 30-min treatment in these two systems and the fluorescence intensities were quite low so that we just can only see the blue background. Therefore, the EEM spectras of water samples in these two systems finally were similar visually, and we labeled the MBO and UV/MBO together at the last sub-graph in Fig. 5. Compared with MBO, the extinction rate of the fluorescence peak in UV/MBO water was significantly faster compared with that in the MBO water. We hypothesize that a greater amount of hydroxyl radicals were generated during UV/MBO and they can enhance the oxidation capacity to remove organic contaminants.

Detection of hydroxyl free radicals and possible mechanisms

The generation of ·OH radicals from ozone plays an important role in purifying polluted river water. This method could improve oxidation effects, as ·OH has a higher oxidation potential than molecular ozone (Agustina et al. 2005). Figure 6 a shows that the fluorescence intensities of the filtered raw river water were used as a blank; there

Fig. 5 EEM spectra of water samples with the reaction time using the MBO and UV/MBO treatments
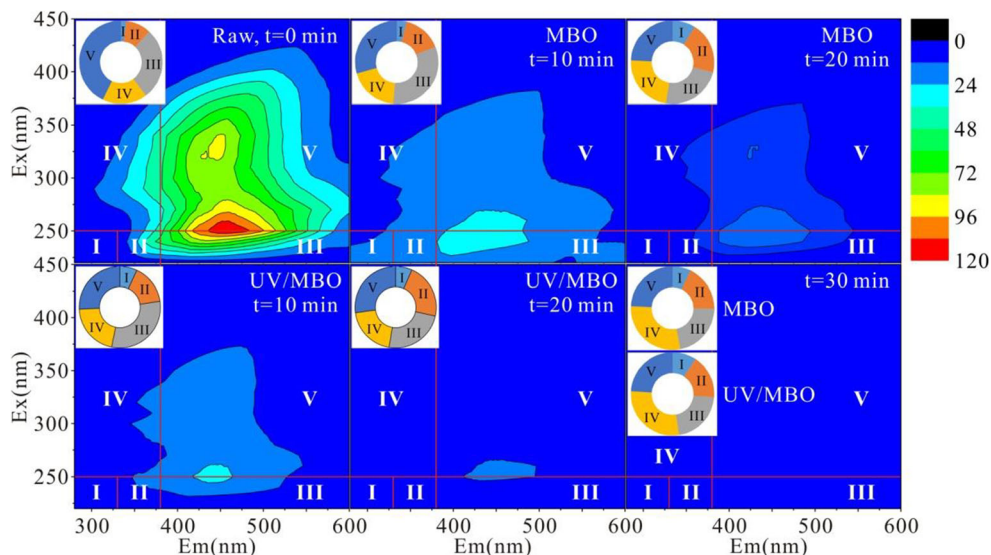

was nearly no fluorescence response at the initial time ($t = 0$ min). After the experiments started, the fluorescence intensities increased with the reaction time under all scenarios. The maximum fluorescence intensities at 30 min were 4.23 ± 0.57, 5.85 ± 0.10, 19.20 ± 0.87, and 24.5 ± 2.04 a.u. with the CO, UV/CO, MBO, and UV/MBO treatments, respectively. Overall, the UV/MBO unit generated ·OH radicals most effectively. The fluorescence response of UV/MBO treated water was almost 5 times stronger than the CO unit.

APF is highly selective; as such, the fluorescence response of APF to ·OH was approximately 133-, 200-, and > 1200-fold greater compared with $^1O_2$, $·O^{2-}$, and H_2O_2, offering good specificity and stability (Setsukinai et al. 2003; Wang et al. 2018). The quantity of generated ·OH can be estimated using an equivalent H_2O_2 concentration, as we observed a linear correlation between the fluorescence intensity and the ·OH concentration produced by H_2O_2 decomposition. Figure 6 b shows the fitted equation as $y = 134.61x$ ($R^2 = 0.9954$). The formula shows that the oxidative capacity of UV/MBO-treated water at $t = 30$ min

was equivalent to 0.18 mM H_2O_2; the values were 0.03, 0.04, and 0.14 mM for CO, UV/VO, and MBO, respectively.

The UV irradiation enhanced ·OH production during ozonation treatment because of the photolysis of ozone (Agustina et al. 2005; Miklos et al. 2018). Microbubbles contributed to a higher ozone solubility, accelerating the reaction rate. Moreover, while the microcosmic mechanism of ·OH generated from micro/nanobubble collapse has been somewhat controversial (Yasui et al. 2018), some experiments have reported that ·OH was detected from liquid water containing bulk micro/nanobubbles in the absence of a dynamic stimulus (Takahashi et al. 2007; Li et al. 2009; Liu et al. 2016). A previous study (Wang et al. 2018) detected ·OH in liquid water containing bulk micro/nanobubbles after generator operations ceased. We speculate that this mechanism also contributed to the ·OH production in this study's MBO and UV/MBO systems. Further study is needed on this topic. However, Fig. 6 b shows that the enhanced ·OH production by UV/MBO was considerable in this study.

Fig. 6 a Fluorescence response of samples at specific times in CO, UV/CO, MBO, and UV/MBO systems indicated by APF and **b** linear correlation between fluorescence increase and H_2O_2 concentrations in the solution
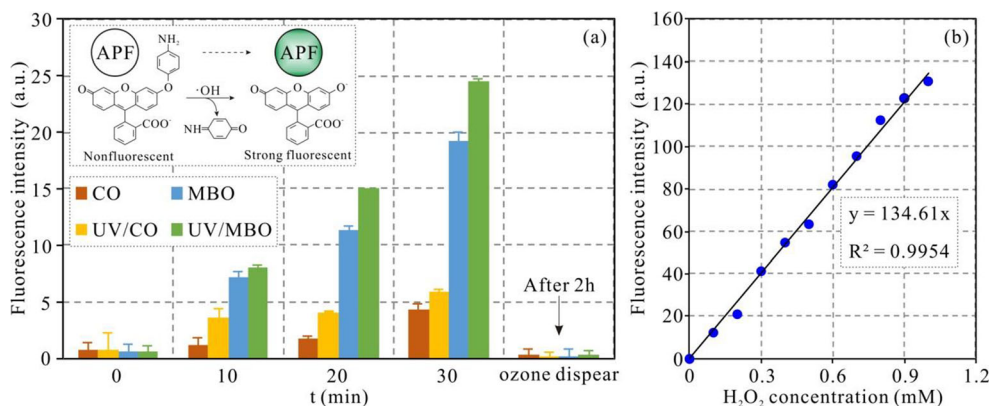
Conclusion

This study investigated an intensified ozonation treatment, using a combination of microbubbles and UV irradiation for the advanced oxidation of those refractory organics. The UV irradiation cleaved the dissolved ozone and generated many ·OH radicals. Microbubbles showed an excellent ability to increase ozone solubility and enhance the mass transfer coefficient; the results were an order of magnitude better than with the conventional macrobubble system at the initial stage. The synergistic effects of UV and microbubbles improved the ozone reaction rate and removal performances of COD, UV_{254}, and UV_{400} in water. The effects also significantly decreased all five categories (regions) of substances according to EEM. This was due to the altered distribution of fractions with different MW values. Organic molecules were oxidized into smaller MW ones, significantly improving the biodegradability of the river water. The enhanced performance of microbubble and UV irradiation was illustrated by the detection and calculation of ·OH radicals using a fluorescent probe method. Overall, intensified ozonation treatment using the combination of microbubble and UV irradiation was determined to improve SE-polluted river water quality, which offers a new strategy for wastewater treatment and environmental remediation.

References

Agustina T, Ang H, Vareek V (2005) A review of synergistic effect of photocatalysis and ozonation on wastewater treatment. J Photochem Photobiol C 6:264–273

Baker JR, Milke MW, Mihelcic JR (1999) Relationship between chemical and theoretical oxygen demand for specific classes of organic chemicals. Water Res 33:327–334

Chen W, Westerhoff P, Leenheer JA, Booksh K (2003) Fluorescence excitation-emission matrix regional integration to quantify spectra for dissolved organic matter. Environ Sci Technol 37:5701–5710

Chiang YP, Liang YY, Chang CN, Chao AC (2006) Differentiating ozone direct and indirect reactions on decomposition of humic substances. Chemosphere 65:2395–2400

Chu L, Yan S, Xing X (2008) Enhanced sludge solubilization by microbubble ozonation. Chemosphere 72:208–212

Cullen PJ, Tiwari BK, O' Donnell CP, Muthukumarappan K (2009) Modelling approaches to ozone processing of liquid foods. Trends Food Sci Technol 20:125–136

Domenjoud B, Tatari C, Esplugas S, Baig S (2011) Ozone-based processes applied to municipal secondary effluents. Ozone-Sci Eng 33:243–249

Ikeura H, Kobayashi F, Tamaki M (2011) Removal of residual pesticides in vegetables using ozone microbubbles. J Hard Mater 186:956–959

Ji X, Zhang W, Jiang M, He J, Zheng Z (2017) Black-odor water analysis and heavy metal distribution of Yitong River in Northeast China. Water Sci Technol 76:2051–2064

Jin X, Peldszus S, Huck PM (2012) Reaction kinetics of selected micropollutants in ozonation and advanced oxidation processes. Water Res 46:6519–6530

Li P, Takahashi M, Chiba K (2009) Enhanced free-radical generation by shrinking microbubbles using a copper catalyst. Chemosphere 77:1157–1160

Liu S, Wang Q, Sun T, Wu C, Shi Y (2012) The effect of different types of micro-bubbles on the performance of the coagulation flotation process for coke waste-water. J Chem Technol Biotehnol 87:206–215

Liu S, Oshita S, Kawabata S, Makino Y, Yoshimoto T (2016) Oxidative capacity of nanobubbles and its effect on seed germination. ACS Sustain Chem Eng 4:1347–1353

Marce M, Domenjoud B, Esplugas S, Baig S (2016) Ozonation treatment of urban primary and biotreated wastewaters: impacts and modelling. Chem Eng J 283:768–777

Miklos DB, Remy C, Jekel M, Linden KG, Drewes JE, Hübner U (2018) Evaluation of advanced oxidation processes for water and wastewater treatment-a critical review. Water Res 139:118–131

Munz NA, Burdon FJ, de Zwart D, Junghans M, Melo L, Reyes M, Schonenberger U, Singer HP, Spycher B, Hollender J, Stamm C (2017) Pesticides drive risk of micropollutants in wastewater-impacted streams during low flow conditions. Water Res 110:366–377

Nishiyama T, Matsuura K, Sato E, Kometani N, Horibe H (2017) Degradation of hydrophilic polymers in aqueous solution by using ozone microbubble. J Photopolym Sci Technol 30:285–289

Özcan A, Özcan AS (2004) Comparison of supercritical fluid and soxhlet extractions for the quantification of hydrocarbons from Euphorbia macroclada. Talanta 64:491–495

Parkinson L, Sedev R, Fornasiero D, Ralston J (2008) The terminal rise velocity of 10-100 μm diameter bubbles in water. J Colloid Interface Sci 322:168–172

Parmar R, Majumder SK (2015) Terminal rise velocity size distribution and stability of microbubble suspension. Asia Pac J Chem Eng 10:450–465

Qiao M, Bai Y, Cao W, Huo Y, Zhao X, Liu D, Li Z (2018) Impact of secondary effluent from wastewater treatment plants on urban rivers: polycyclic aromatic hydrocarbons and derivatives. Chemosphere 211:185–191

Saeed T, Paul B, Afrin R, Al-Muyeed A, Sun G (2016) Floating constructed wetland for the treatment of polluted river water: a pilot scale study on seasonal variation and shock load. Chem Eng J 287:62–73

Setsukinai K, Urano Y, Kakinuma K, Majima HJ, Nagano T (2003) Development of novel fluorescence probes that can reliably detect reactive oxygen species and distinguish specific species. J Biol Chem 278:3170–3175

Takahashi M, Chiba K, Li P (2007) Free-radical generation from collapsing microbubbles in the absence of a dynamic stimulus. J Phys Chem B 111:1343–1347

Tambo N, Kamei T (1978) Treatability evaluation of general organic matter. Matrix conception and its application for a regional water and waste water system. Water Res 12:931–950

Temesgen T, Bui TT, Han M, Kim T, Park H (2017) Micro and nanobubble technologies as a new horizon for water-treatment techniques: a review. Adv Colloid Interface Sci 246:40–51

Tripathi S, Pathak V, Tripathi DM, Tripathi BD (2011) Application of ozone based treatments of secondary effluents. Bioresour Technol 102:2181–2186

von Sonntag C (2008) Advanced oxidation processes: mechanistic aspects. Water Sci Technol 58:1015–1021

Wang WT, Fan W, Huo MX, Zhao HF, Lu Y (2018) Hydroxyl radical generation and contaminant removal from water by the collapse of

microbubbles under different hydrochemical conditions. Water Air Soil Poll 229:86–97

Xing Y, Yu Y, Men Y (2018) Emerging investigators series: occurrence and fate of emerging organic contaminants in wastewater treatment plants with an enhanced nitrification step. Environ Sci Water Res Technol 4:1412–1426

Yao K, Chi Y, Wang F, Yan J, Ni M, Cen K (2016) The effect of microbubbles on gas-liquid mass transfer coefficient and degradation rate of COD in wastewater treatment. Water Sci Technol 73:1969–1977

Yasui K, Tuziuti T, Kanematsu W (2018) Mysteries of bulk nanobubbles (ultrafine bubbles): stability and radical formation. Ultrason Sonochem 48:259–266

Zhao X, Hu HY, Yu T (2014) Effect of different molecular weight organic components on the increase of microbial growth potential of secondary effluent by ozonation. J Environ Sci 26:2190–2197

Zheng T, Wang Q, Zhang T (2015) Microbubble enhanced ozonation process for advanced treatment of wastewater produced in acrylic fiber manufacturing industry. J Hazard Mater 287:412–420

Zimmerman WB, Tesař V, Hemaka Bandulasena HC (2011) Towards energy efficient nanobubble generation with fluidic oscillation. Curr Opin Colloid Interface Sci 16:350–356